Supplementary Material

Quasi-One-Dimensional Metal-Insulator Transitions in Compound Semiconductor Surfaces

J. Z. Zhao[1,2], W. Fan[3], M. J. Verstraete[4], Z. Zanolli[5,6], J. Fan[1], X. B. Yang[7], H. Xu*[1], and S. Y. Tong*[1,8]

1 Department of Physics, South University of Science and Technology of China, 518055 Shenzhen, People's Republic of China

2 Dalian Institute of Chemical Physics, Chinese Academy of Sciences, 116023 Dalian, People's Republic of China

3 Computational Condensed Matter Physics Laboratory, RIKEN ASI, Wako, Saitama 351-0198, Japan

4 Département de Physique and European Theoretical Spectroscopy Facility, Universite de Liège, B-4000 Sart Tilman, Liège, Belgium

5 Peter Grünberg Institute (PGI-1) and Institute for Advanced Simulation (IAS-1), Forschungszebtrum Jülich, D-52425 Jülich, Germany

6 Institute for Theoretical Solid State Physics and European Theoretical Spectroscopy Facility (ETSF), RWTH Aachen University, D-52056 Aachen, Germany

7 Department of Physics, South China University of Technology, Guangzhou 510640, People's Republic of China

8 School of Science and Engineering, The Chinese University of Hong Kong (Shenzhen), 518172 Shenzhen, People's Republic of China

August 23, 2016

Contents

S1 Further discussion on the experimental feasibility

The adsorption energy per X species (H or Li) is calculated as:

$$E_{ads} = (E_{total} - E_{bare} - nE_X)/n$$

E_{total} is the total energy of the system, E_{bare} is the energy of the stoichiometric surface, E_X is the energy of the X species (from atomic to the most stable form), and n is the number of X species in a unit cell.

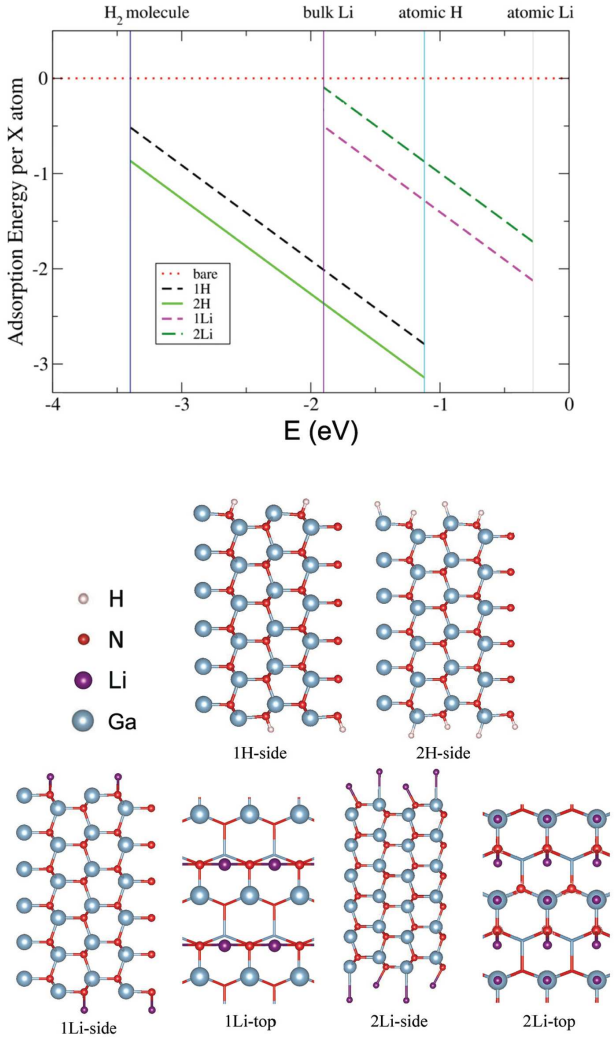

FIG. S1: (Color online). Binding energy for $GaN(10\bar{1}0)$-$1H$, $GaN(10\bar{1}0)$-$2H$, $GaN(10\bar{1}0)$-$1Li$ and $GaN(10\bar{1}0)$-$2Li$ phases.

Fig. S1 shows that $GaN(10\bar{1}0)$-$2H$ is always more stable than $GaN(10\bar{1}0)$-$1H$. However, the barrier for the phase transition from $1H$ to $2H$ (see FIG. S2) is around $1eV$. The transition barrier is somewhat large, so it seems reasonable to observe $GaN(10\bar{1}0)$-$1H$ experimentally.

Li prefers to bind to two surface *N* atoms, so that $GaN(10\bar{1}0)$-*1Li* is the most stable energetically, which indicates that the $GaN(10\bar{1}0)$-*1Li* structure should be a suitable system to study Peierls transition experimentally.

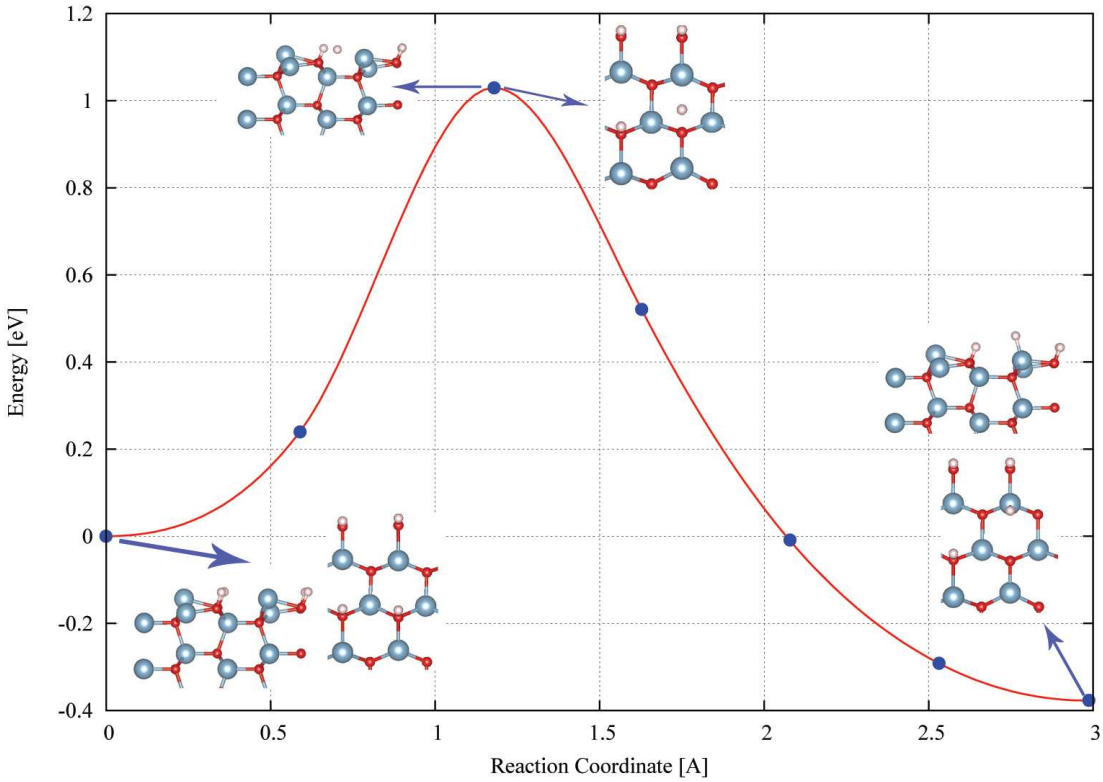

FIG. S2: (Color online). The calculated reaction path from $GaN(10\bar{1}0)$-*1H* to $GaN(10\bar{1}0)$-*2H* phase, shown in side and top view in the inset.

S2 Electronic bands and DOS of $GaN(10\bar{1}0)$-*1Li*

The electronic behaviors of $GaN(10\bar{1}0)$-*1Li* are similar to the ones of $GaN(10\bar{1}0)$-*1H*, and they support the same conclusions described in the main text.

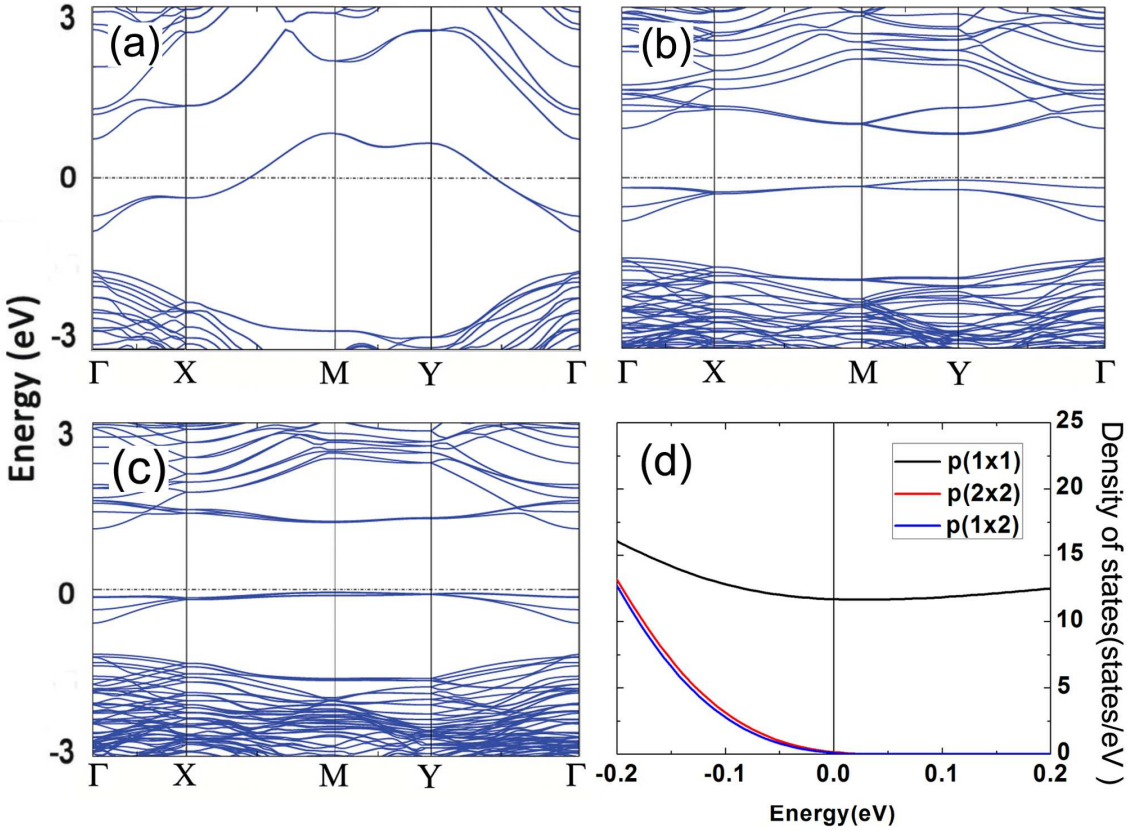

FIG. S3: (Color online). The calculated electronic band structures and density of states (DOS) of the different phases of $GaN(10\bar{1}0)$-*1Li* (all slabs have 12 layers). The Fermi energy is set to zero. The band structures of p(1 × 2) and p(2 × 2) phase are calculated in a p(2 × 2) cell. (a) $p(1\times1)$, (b) $p(2\times2)$ and (c) $p(1\times2)$ phase, (d) The DOS of $p(1\times1)$, $p(1\times2)$ and $p(2\times2)$ phases.

S3 Projected Density of State for p(1×1)

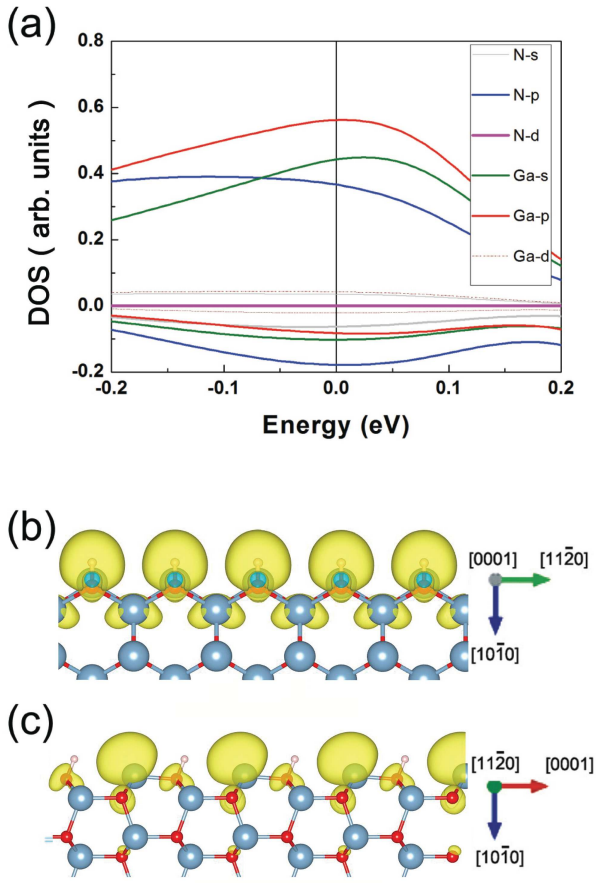

FIG. S4: Electronic properties of the p(1×1) surface cell: (a) Density of states projected on surface atoms, with the Fermi energy set to zero. (b and c) The isosurface of probability density for the surface bands near E_F (between -0.05 eV and E_F), along [0001] (b) and [11$\bar{2}$0] (c). The isosurface value is 3×10^{-4} $e/bohr^3$. The states form continuous modulated tubes of electron density following Ga atom chains along [11$\bar{2}$0], and discontinuous pockets following chains of Ga and N atoms along [0001].

S4 Charge redistribution analysis

We carried out the Bader charge analysis for both $GaN(10\bar{1}0)$-*1H* and $GaN(10\bar{1}0)$-*1Li* system. The results indicate that the essential charge redistributions occur between surface Ga atoms displaced upwards (charge donors) to the surface Ga atoms displaced downwards (charge acceptors). The charge on the inner atomic layers remains practically the same for the three phases. The charge on surface N and H/Li also remains essentially unaffected. The results confirm that there is little charge transfer between the layers, which indicates little 3D charge redistribution effects during the MI transition.

TABLE SI: Charge transfer obtained by Bader charge analysis (in e) for p(1 × 1), p(1 × 2) and p(2 × 2) phase for 12-layer slab of wurtzite $GaN(10\bar{1}0)$-*1H*. In the layer 1 of reconstructed phases, the Ga_u (resp. Ga_d) refers to the Ga moving upwards (resp. downwards) in the buckling distortions.

	p(1 × 1)			p(1 × 2)			p(2 × 2)		
	Ga	N	H	Ga	N	H	Ga	N	H
layer-1	+1.00	-1.57	+0.39	+0.58(Ga_u) +1.44(Ga_d)	-1.56	+0.40	+0.57(Ga_u) +1.44(Ga_d)	-1.55	+0.42
layer-2	+1.54	-1.50		+1.53	-1.47		+1.55	-1.50	
layer-3	+1.52	-1.47		+1.51	-1.47		+1.51	-1.47	
layer-4	+1.53	-1.47		+1.53	-1.49		+1.52	-1.47	
layer-5	+1.53	-1.47		+1.53	-1.47		+1.52	-1.47	
layer-6	+1.53	-1.47		+1.53	-1.47		+1.53	-1.47	

TABLE SII: Charge transfer obtained by Bader charge analysis (in e) for p(1 × 1), p(1 × 2) and p(2 × 2) phase for 12-layer slab of wurtzite $GaN(10\bar{1}0)$-*1Li*. In the layer 1 of reconstructed phases, the Ga_u (resp. Ga_d) refers to the Ga moving upwards (resp. downwards) in the buckling distortions.

	p(1 × 1)			p(1 × 2)			p(2 × 2)		
	Ga	N	Li	Ga	N	Li	Ga	N	Li
layer-1	+0.89	-1.72	+0.86	+0.60(Ga_u) +1.36(Ga_d)	-1.72	+0.86	+0.58(Ga_u) +1.37(Ga_d)	-1.69	+0.86
layer-2	+1.49	-1.52		+1.50	-1.52		+1.52	-1.52	
layer-3	+1.53	-1.54		+1.54	-1.55		+1.53	-1.54	
layer-4	+1.54	-1.54		+1.54	-1.54		+1.54	-1.54	
layer-5	+1.54	-1.54		+1.55	-1.55		+1.54	-1.54	
layer-6	+1.54	-1.54		+1.54	-1.54		+1.53	-1.54	

S5 Atomic displacement of $GaN(10\bar{1}0)$-*1H*

Our calculations show that over 90% of the distortions are confined to the rows of surface *Ga* atoms, mirroring closely the confinement of charge redistributions. This evidence, together with the results from charge redistribution analysis, confirms that such MI transition is confined to the surface 1D atom chain without affecting the inner layers.

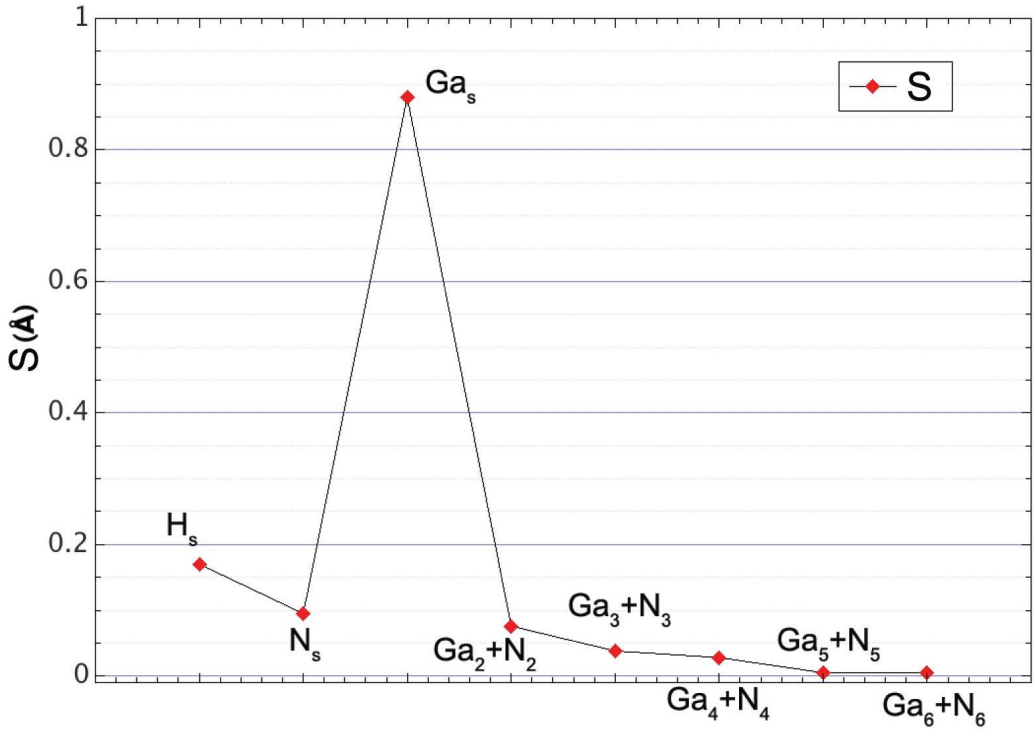

FIG. S5: (Color online). Sum of absolute displacement of the atomic reconstruction of the p(2×2) $GaN(10\bar{1}0)$-*1H* with respect to the p(1×1) phase. The subscript n of each atomic symbol indicates the corresponding layer, while s refers to the surface. For surface atoms, S is the sum of the absolute value of displacements of all the atoms of the same kind. For the inner layers, S is the sum of the absolute value of the displacements of one *Ga* and one *N* belonging to the same layer.

S6 Instabilities of p(1×1) *ZnO*$(10\bar{1}0)$-*1H*

The presence of many phonon modes with imaginary frequency in the phonon dispersion curve and the corresponding Fermi surface show that the p(1×1) phase of *ZnO*$(10\bar{1}0)$-*1H* is unstable. The situation is analogous to the p(1×1) phase of *GaN*$(10\bar{1}0)$-*1H*.

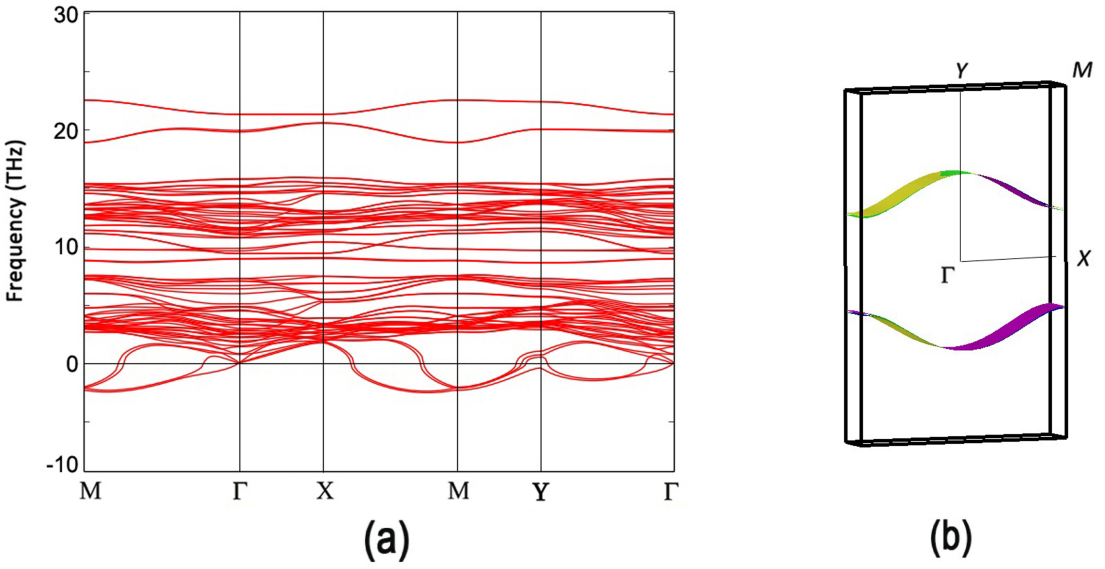

FIG. S6: (Color online) (a) Phonon dispersion curves of a p(1×1) 12-layer slab of *ZnO*$(10\bar{1}0)$-*1H*. The phonon frequencies are in units of *THz*. The negative values refer to unstable phonon modes. (b) The 2D Fermi surface of the p(1×1) 12-layer slab of *ZnO*$(10\bar{1}0)$-*1H*. The origin is taken at the center of the BZ.

S7 Electronic Band Structures and DOS of $ZnO(10\bar{1}0)$-*1H* and $ZnO(10\bar{1}0)$-*1Li*

Similar to the case of *GaN* series systems, the electronic band structures of $ZnO(10\bar{1}0)$-*1H* $p(1 \times 1)$ phase shows its conductivity while a sizable band gap is opened at the Fermi level in $p(2 \times 2)$ phase. Comparison of the DOS near the Fermi level shows that the charge close to the Fermi level moves to lower energy levels when the band gap opens going from the $p(1 \times 1)$ to the $p(2 \times 2)$ phase, as predicted in a Peierls transition.

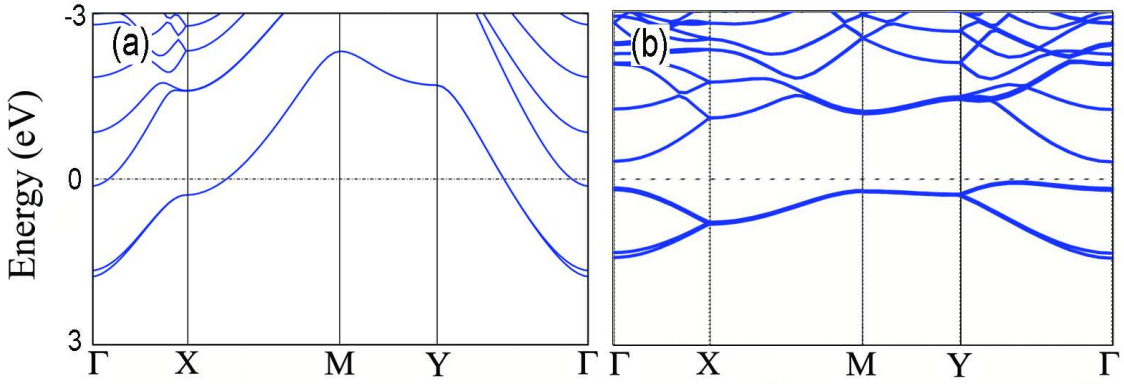

FIG. S7: (Color online). The calculated electronic band structures of the different phases of $ZnO(10\bar{1}0)$-*1H* (all slabs have 12 layers). (a) The band structure of $p(1 \times 1)$ phase. (b) The band structure of $p(2 \times 2)$ phase.

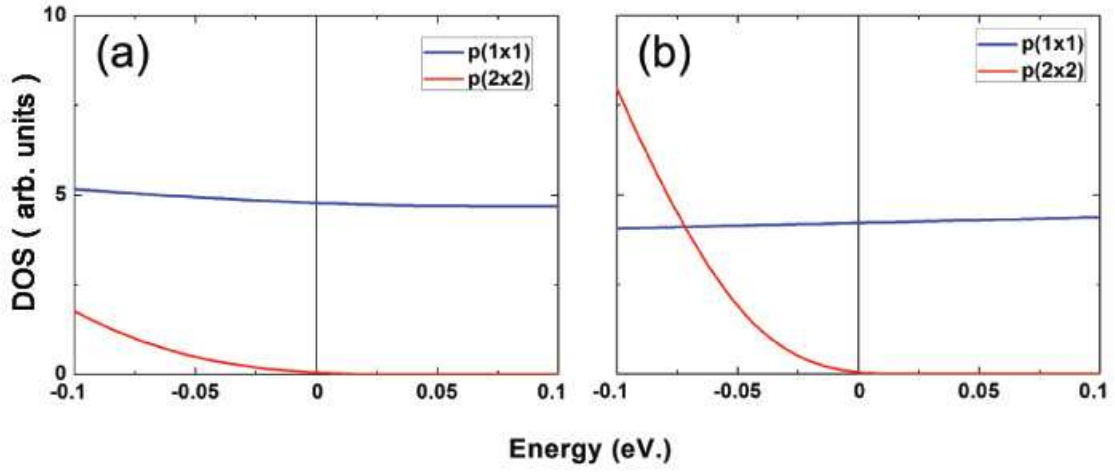

FIG. S8: (Color online). The calculated DOS of the different phases of $ZnO(10\bar{1}0)$-*1H* and $ZnO(10\bar{1}0)$-*1Li* (all slabs have 12 layers). (a) The DOS of $p(1 \times 1)$ and $p(2 \times 2)$ phases of *1H*. (b) The DOS of $p(1 \times 1)$ and $p(2 \times 2)$ phases of *1Li*.

S8 Surface stabilization of $\boldsymbol{AlN}(10\bar{1}0)$-*1H* and $\boldsymbol{BeO}(10\bar{1}0)$-*1H*

Peierls type MI transition occurs in $AlN(10\bar{1}0)$-*1H* and $BeO(10\bar{1}0)$-*1H* systems. The surface stabilization energy gain are listed in Table SIII. Both of them undergo dimerization type atomic distortion in which atom moves longitudinally against each neighbor forming two atoms pair. Accompanying bandgap opening, the symmetry of $AlN(10\bar{1}0)$-*1H* changes from $p(1 \times 1)$ to $p(2 \times 2)$ while the symmetry of $BeO(10\bar{1}0)$-*1H* changes from $p(1 \times 1)$ to $p(1 \times 2)$.

TABLE SIII: Surface stabilization energy (ΔE), electronic band-gap for a 12-layer slab of wurtzite *AlN-1H*, and *BeO-1H*. The surface stabilization energy is the energy gained due to surface reconstruction per p(2×2) cell, i.e. the difference between the total energy of the reconstructed surface ($E_{recon.}$) and the non-reconstructed surface ($E_{non.}$).

	Cell	$\Delta E(eV)$	Gap(eV)
$AlN(10\bar{1}0)$-*1H*	2×2	-0.07	0.37
$BeO(10\bar{1}0)$-*1H*	1×2	-0.10	0.40